Theoretical and experimental study on ultrasonic dispersion of nanoparticles for strengthening cast Aluminum Alloy A356

*Xiaochun Li, *Yong Yang, **David Weiss
*University of Wisconsin-Madison, Madison, WI
**Edk Industries Inc, Manitowoc, WI

ABSTRACT

Aluminum alloy A356 is of significance for numerous applications. The mechanical properties of A356 would be enhanced considerably if reinforced by thermo-dynamically-stable nanoparticles. However, it is very challenging to disperse nanoparticles uniformly in A356 melts for casting A356 nanocomposites. In this study, ultrasonic cavitation effect was proposed to disperse SiC nanoparticles in A356 melts before casting. The novel method was theoretically studied and then experimented. With only 1.0wt.% nano-sized SiC reinforcement (about 30nm), the ultimate tensile strength and yield strength of the aluminum alloy A356 were enhanced significantly while the ductility was retained. The study on micro/nano structures of the nanocomposites validates that a uniform distribution and effective dispersion of nanoparticles in A356 matrix were achieved. Moreover, a good bonding between the SiC nanoparticles and the Al matrix was obtained. This study paves a way for high volume solidification processing of metal matrix nanocomposites for industrial applications.

RIASSUNTO

La lega di alluminio A356 è correntemente utilizzata in numerose applicazioni. Le proprietà meccaniche di questa lega possono essere notevolmente migliorate per indurimento mediante nanoparticelle termodinamicamente stabili. Tuttavia ottenere un nanocomposito disperdendo le nanoparticelle in modo uniforme nella lega A356 allo stato fuso è piuttosto impegnativo. In questo studio, per disperdere nanoparticelle di SiC nella lega fusa prima della colata, è stato utilizzato il meccanismo della cavitazione prodotta da ultrasuoni. Questo nuovo procedimento è stato studiato teoricamente e poi sperimentalmente. Con l'aggiunta di appena l'1.0% in peso di nanoparticelle di SiC (30nm circa) è stato ottenuto, a parità di duttilità, un significativo incremento sia dello sforzo tensile critico (UTS) sia dello sforzo di snervamento. L'analisi strutturale di campioni di lega, condotta su scala microscopica e su scala nanoscopica, conferma che è stata effettivamente raggiunta una distribuzione uniforme delle nanoparticelle di SiC nella matrice di A356. Il metodo innovativo proposto in questo lavoro consente di ottenere grandi volumi di nanocompositi a matrice metallica per le applicazioni industriali.

KEYWORDS

Ultrasonic cavitation, Aluminum alloy A356, Nanocomposite, and casting.

INTRODUCTION

In recent years, significant effort has been taken to develop metal matrix nanocomposites (MMNCs) [1-12]. Compared with conventional metal matrix composites (MMCs) that are reinforced with micro inclusions, this new class of material can overcome many disadvantages in MMCs [13-14], such as poor ductility, low fracture toughness and machinability. The properties of metals would be enhanced considerably if reinforced by ceramic nanoparticles (less than 100nm). Moreover, MMNCs could offer a significantly improved performance at elevated temperatures [7-10]. MMNCs are poised to generate enormous impact on aerospace, automobile, and military industries.

Although MMNCs have a great potential for widespread applications, the current processing technologies are neither reliable nor cost effective to enable a high volume and net shape production of complex MMNC structural components with reproducible structures and properties. Traditional fabrication methods, such as high energy ball milling, rapid solidification, electroplating, and sputtering etc, can not be used for mass production and net shape fabrication of complex structural components without significant post processing [7-12].

In this research, a new method that combines solidification processes with ultrasonic cavitation based dispersion of nanoparticles in metal melts has been

developed. Ultrasonic cavitation can produce transient (in the order of nanoseconds) micro "hot spots" that can have temperatures of about 5000ºC, pressures above 1000 atms, and heating and cooling rates above 1010 K/s [15]. The strong impact coupling with local high temperatures can potentially break the nanoparticle clusters and clean the particle surface. Since the nanoparticle clusters are loosely packed together, air could be trapped inside the voids in the clusters, which will serve as nuclei for cavitations. The size of clusters ranges from nano to micro due to the attraction force among nanoparticles and the poor wettability between the nano particles and metal melt.

MATERIAL SYSTEM SELECTION

For conventional MMCs, aluminum, titanium and magnesium are the prevalent matrix materials and the reinforcement is frequently accomplished using boron, graphite or SiC fibers, particulates, or whiskers etc. To select a suitable reinforcement and matrix for the aluminum nanocomposite, important factors such as density, wettability and chemical reactivity at high temperatures should be considered. For conventional Al-based MMCs, SiC is a popular reinforcement because of its relatively good wettability to aluminum alloys and nearly identical density to that of Al alloys [16]. However SiC is thermodynamically unstable in molten aluminum at temperatures above 727 °C since SiC can react with molten aluminum to form Al4C3, releasing silicon into the matrix [17]. However, this reaction can be significantly suppressed by using a matrix alloy containing a high Si content. An addition of 7wt.% Si can effectively suppress the reaction below 800°C, although it is slightly below the optimum silicon content level for a complete stability. Based on the above considerations, A356 aluminum alloy is a suitable matrix material to prevent the formation of Al4C3. And for SiC nanoparticles, oxidation occurs easily to form a SiO2 thin layer in angstrom scale on the particle surface. This oxide layer can prevent a further reaction between SiC and Al melt during processing [18]. Moreover, aluminum alloy A356 was selected as the matrix material since it is also readily castable and widely studied. The chemical composition of the A356 alloy is shown in Table 1. The nano-sized ceramic particles used in this study were _-SiC (spherical shape, average diameter<=30nm, Composition: SiC>=95%, [O]:1~1.5%, [C]: 1~2%).

Table 1 Nominal Chemical Composition of Matrix Alloy A356 (wt%)

Si	Fe	Cu	Mn	Mg	Zn	Ti	Al
6.5-7.5	0.20	0.20	0.10	0.25-0.45	0.10	0.20	bal

THEORETICAL STUDY

It is envisioned that strong micro scale transient cavitations can effectively distribute and disperse nanoparticles into alloy melts and also enhance their chemical reactivity and wettability, thus making the solidification processing of high performance lightweight metal nanocomposites feasible [19, 20]. The action of ultrasonic in melt metal is not yet completely understood, although most researchers invoke a mechanism in which cavitation plays a key role in increasing the number of nucleation centers [15].

To initiate the fundamental study of nanoparticle dispersion by ultrasonic cavitation, a simplified model was used: two nanoparticles entrapped inside aluminum melt, as shown by Fig. 1. There are two forces that hold two nanoparticles together in the melt: intrinsic van der Waals force and capillary force applied by the melt surface tension. These two forces vary with the separation distance between these

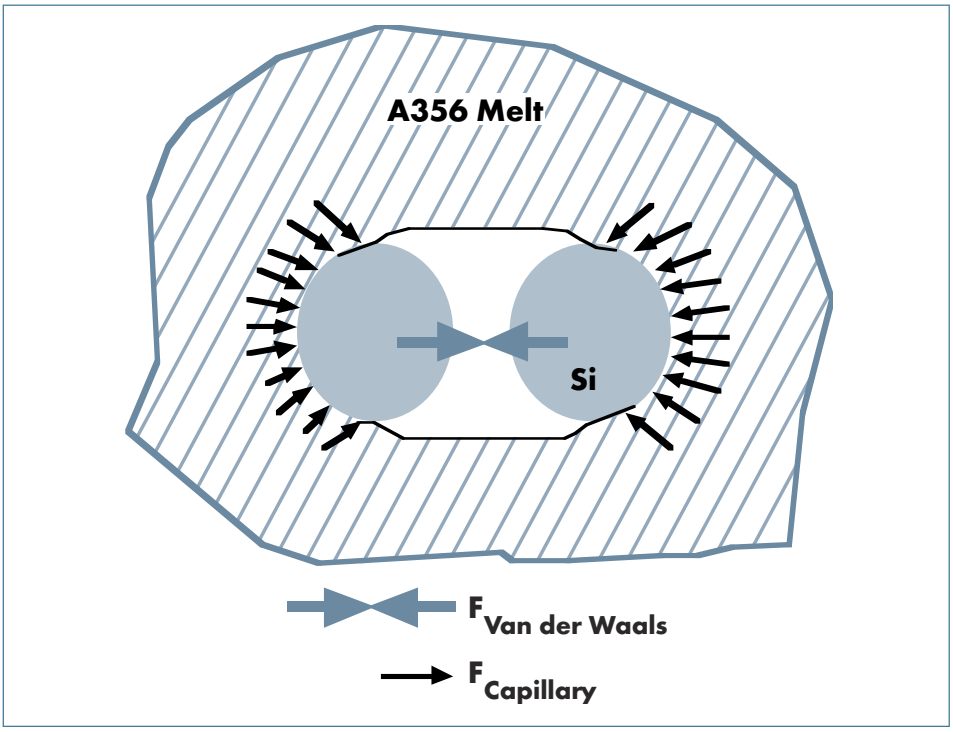

Fig. 1: Model for dispersion of two SiC nanoparticles in aluminum alloy melt.

two particles. In this model, the maxima of these two forces were estimated separately and then added together to derive the maximum pressure required to separate the two nanoparticles, that is, to disperse them. To calculate the Van der Waals force, the Lennard-Jones potential model is employed, first the potential energy of the two attracted particles is obtained vs. the distance between them, and then the derivative of the potential is calculated to obtain the force between these two particles.

$$\text{Potential} = \int_{v1} dV_1 \int_{v2} q^2 V(r) dV_2 \qquad \text{Eq. (1)}$$

Where dV_1 and dV_2 are the infinitesimal volume elements in the particles of volume V_1 and V_2, respectively. As depicted in Fig. 2, r is the distance between the volume elements dV_1 and dV_2, q is the molecule density and V(r) is the inter-molecular potential defined as Lennard-Jones potential model.

Eq.1 was numerically integrated and the Van der Waals force was calculated as the derivative of potential and plotted in Fig.3, where attractive forces are denoted as positive values and repulsive forces are negative values. As the radius of the nanoparticles varies from 1 nm to 100 nm, the force also increases. For the SiC nanoparticles with a radius of 15 nm, the maximum van der Waals force is approximately 40 nN.

Due to the poor wettability between the SiC nano particles and the Al melt [16, 21], the nanoparticle/melt system to estimate the capillary force applied by the Al melt should be considered as hydrophobic. As shown in Fig. 4, the force generated by the melt surface tends to push the particle out of the melt; this force is called capillary force, F_c, and given by:

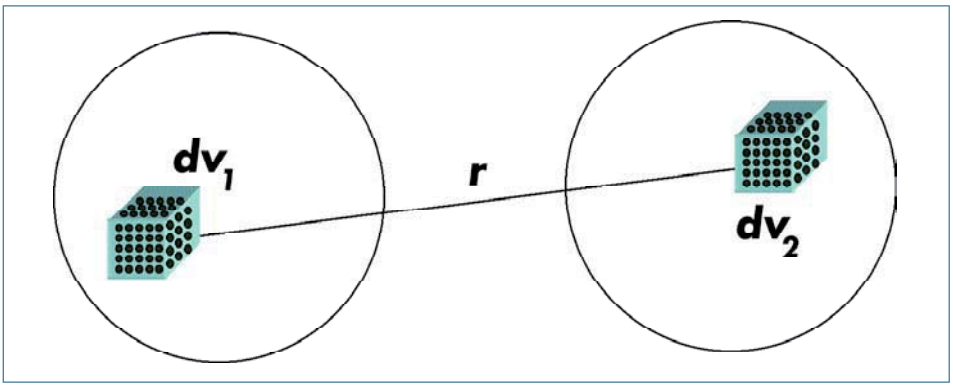

Fig. 2: Schematic representation of interaction of ultra-fine particles (not to scale).

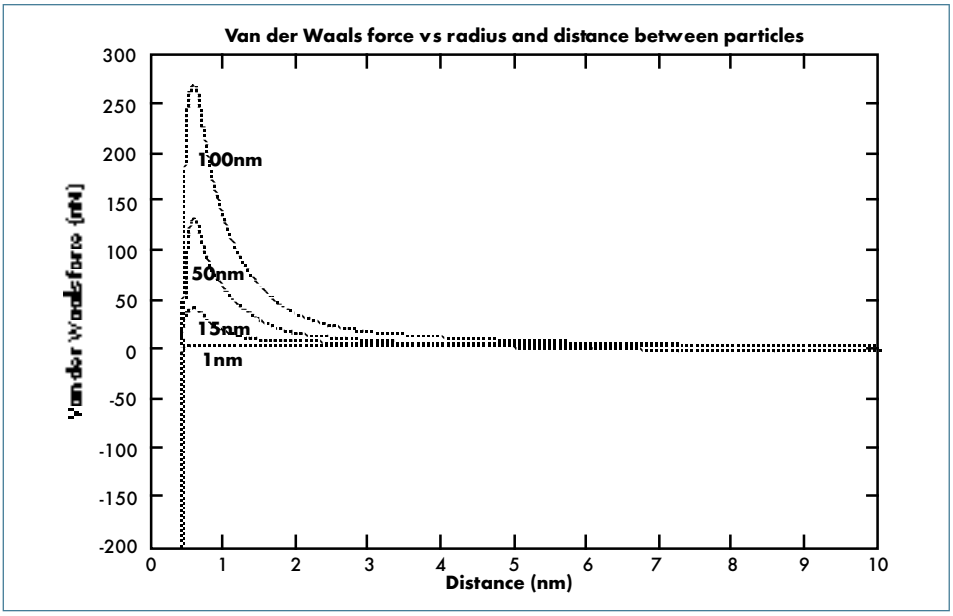

Fig. 3: Vander waals force vs. SiC nanoparticle separation distance.

$$Fe = 2\pi(R \sin\theta_c)\gamma \sin[\theta_c - (\pi - \alpha)] = -2\pi(R \sin\theta_c)\gamma \sin(\theta_c + \alpha) \qquad \text{Eq. (2)}$$

Where, d is the diameter of the nanoparticle, the contact angle α =127° [21], γ is the surface tension coefficient, and θ_c is the filling angle, which is a function of the contact angle. Then the maximum capillary force was calculated to be approximately 16nN.

Therefore, for the SiC nanoparticles with a radius of 15 nm, the maximum total attraction force is approximately 56nN. The minimum pressure, P_{min}, generated by the bubble in order to separate the two SiC nanoparticles with a radius of 15 nm can be estimated as:

$$P = F_{attraction} / A_{effective} = 56\times10^{-9} / (\pi \times 15^2 \times 10^{-18}) = 65\text{MPa} = 650\text{atm} \qquad \text{Eq. (3)}$$

In order to compare the pressure generated by ultrasonic cavitation with the required minimum pressure for the SiC nanoparticle dispersion (separation), a simple model involving a single cavitation bubble in the Al melt was studied. For an isolated cavitation bubble with a radius R, where R = R(t), executing pulsations in an ideal incompressible liquid, with pressure p and velocity u in the liquid at a point r in space, where , at time t, we have the equation of motion [19], described as a second-order nonlinear differential equation.

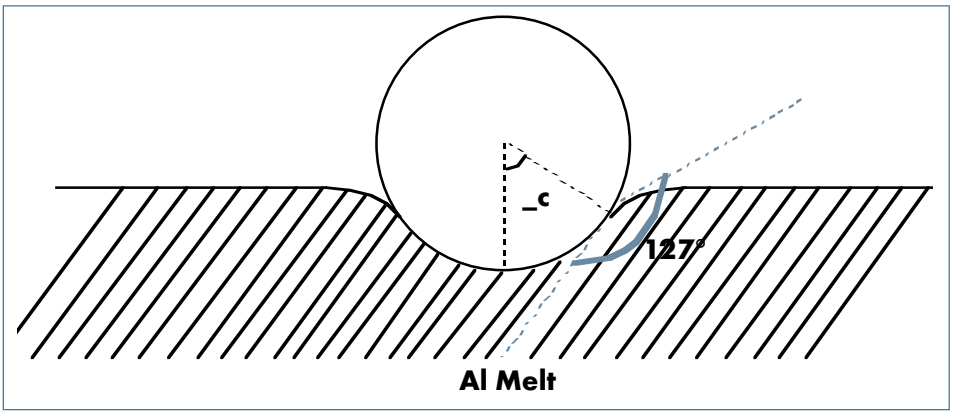

Fig. 4: Hydrophobic model for the nano SiC particle with Al melt.

$$R\frac{d_2 R}{dt_2}+\frac{3}{2}\left(\frac{dR}{dt}\right)^2+\frac{1}{\rho_0}\left[p_0-p_v-p_m\sin\omega t+\frac{2\sigma}{R}-\left(p_0+\frac{2\sigma}{R_0}\right)\left(\frac{R_0}{R}\right)^{3\gamma}\right]=0 \qquad \text{Eq. (4)}$$

Where R_0 is the initial bubble radius, and p_0, p_v, p_m are atmosphere pressure, bubble vapor pressure and ultrasonic field pressure, respectively. The numerical solution for R(t) was obtained in Matlab® with the Runge-Kutta fourth order method, with initial conditions:

R_0 = 100μm and 1μm;

f = 17500Hz and $\varpi = 2\pi f = 2\pi * 17500$;

p_0 = 1atm;

p_m = 3.7 MPa (output of the ultrasonic transducer to be used in this study);

Surface tension σ = 0.072m/s when aluminum melt is at 680 °C

The $R(t)/R_0$ for different radius is plotted in Fig.5a for the initial bubble size R_0=100μm and Fig.5b for R_0=1mm. During the collapse of a cavitation bubble, the pressure on its surface can be extremely high. The bubble radiates spherical waves of finite amplitudes, which are converted into shock waves into the liquid, generating the cavitation phenomena. The cavitation pressure was calculated with Green function and also plotted in Fig.5a for R_0=100μm and Fig.5b for R_0=1μm.

From Fig.5 (a) and (b), the plot suggests that, as the initial radius decreases, the cavitations pressure increases dramatically. From our preliminary studies [22], it was found the size of nanoparticle clusters mainly varies from 1μm to 100μm. For bubbles with this range of initial radius, the cavitation pressure can reach up to 6,000atms, which is significantly higher than the required minimum bubble pressure (650 atms from Eq.3) to separate the two SiC nanoparticles with a diameter of 30nm. The theoretical study suggests that the acoustic cavitations can generate adequate pressure to break SiC nanoparticle clusters in aluminum melt.

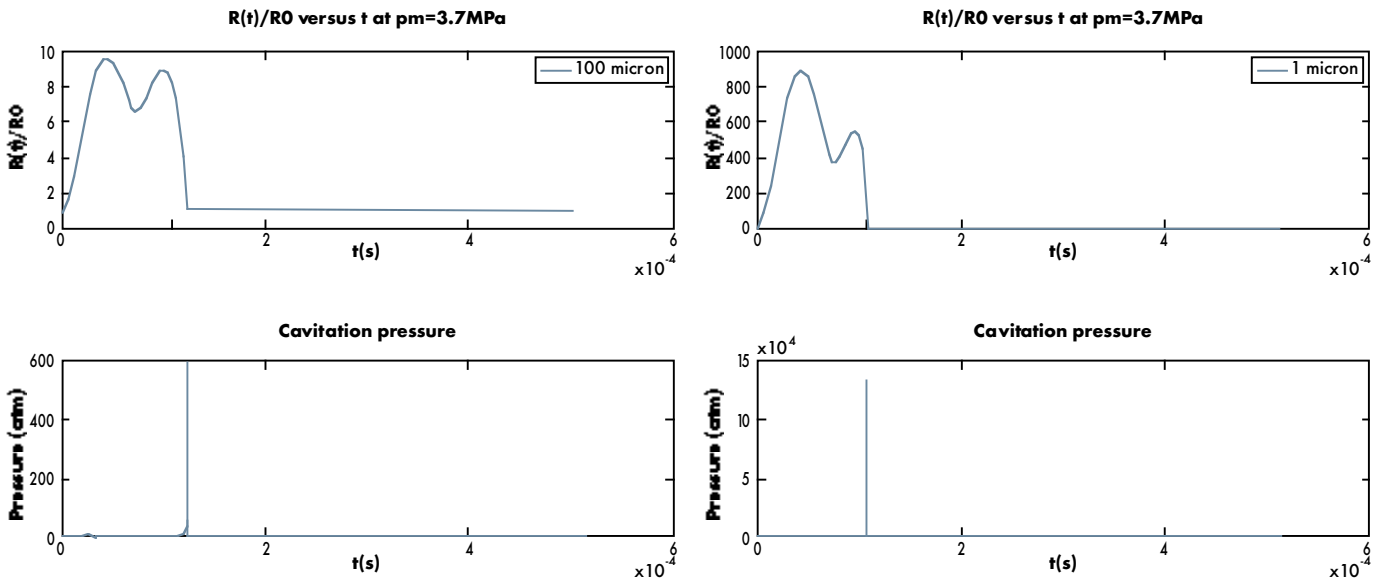

(a) Bubble initial radius at 100μm

(b) Bubble initial radius at 1μm

Fig. 5: Cavitation pressures vs. initial bubble radius

EXPERIMENTAL SETUP AND PROCEDURE

As shown in Fig.6, the experimental setup consisted of processing and controlling parts. An electric resistance heating unit was used to melt the A356 in a small graphite crucible with a casting capacity of approximately 2 lbs, controlled with an electric transformer. A Permendur power ultrasonic probe with Niobium waveguide, coupled to a 17.5 kHz and maximum 4.0 kW power output from a controller unit (Advanced Sonics, LLC, Oxford, CT), was dipped into the melt for ultrasonic processing. This ultrasonic machine would generate a maximum ultrasonic intensity of 125W/cm2 at the end of the niobium tip. The Al melt was protected with four Argon shield gas nozzles. The processing temperature was monitored with a steel sheathed thermocouple probe. Nano-sized SiC particles were added into melts from the top of crucible during the process.

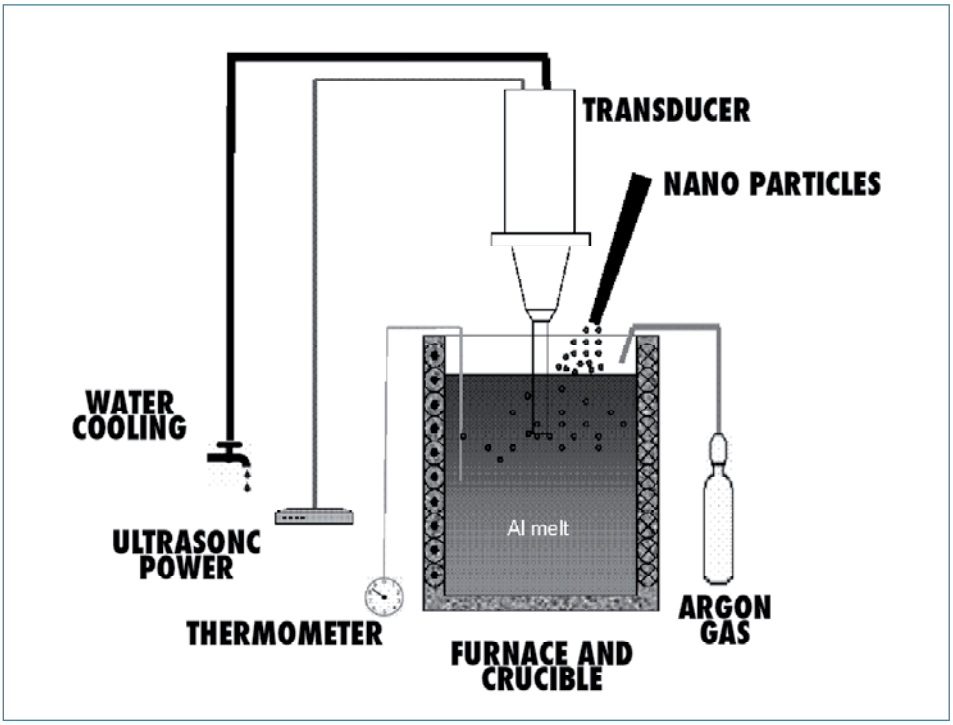

Fig. 6. Schematic of experimental setup.

The A356 alloy was first melted in a crucible with 50lb capacity by an induction furnace, and some of the molten alloy was then transferred to the processing graphite crucible. Before the ultrasonic probe was dipped in, the melt was treated with a mixture gas (99% nitrogen and 1% chorine) for about 3 minutes to eliminate as much oxide and hydrogen as possible. To cast high quality tensile specimen, steel mold was selected because it can offer good complexity, high cooling rate, and smooth casting surface. The mold was designed and fabricated according to ASTE (ASTM B 108-03a). An additional graphite pouring cup was assembled to guide the melt and serve as housing for the ceramic filter. With SiC nanoparticles added into the melt, the viscosity of the melt increased significantly. However, after adequate ultrasonic processing, the viscosity of the melt decreased, but still higher than that of a pure alloy melt. In order to improve the flowability during casting, a higher casting temperature of 780°C was used. The steel mold was preheated to 350°C with a torch to ensure that the melt would fill the mold fully.

The ultrasonic processing temperature was controlled at between 50 °C and 150 °C above the A356 alloy melting point (610 °C). To optimize the processing parameters, Design of Experiments (DOE) method was used. For DOE, different ultrasonic power levels and different processing temperatures were tested. The processing time was controlled at 60 minutes inside the graphite crucible.

All cast nanocomposite specimens were T6 heat treated to be comparable with the industrial standard (Heat Treating Engineers Inc, Milwaukee). To test the mechanical properties of the MMNCs, specimens with a diameter of 0.35 inch (8.89mm) and a gage length of 1.25 inch (31.75mm) were tested on a Sintech 10/GL with an extensometer.

For micro/nano structure study, samples of bulk MMNCs were cut and mounted with epoxy, and mechanically polished down to 0.05μm surface finish. Scanning Electron Microscopy (SEM) images were obtained with LEO1530. Transmission Electron Microscopy (TEM) Philips CM200 equipped with Energy Dispersion Spectrum (EDS) was used to study the nanostructure of MMNCs, such as local dispersion, interfacial bonding, and chemical composition.

RESULTS AND DISCUSSION

PROCESSING PARAMETER OPTIMIZATION THROUGH DESIGN OF EXPERIMENT (DOE)

To optimize the processing parameters, design of experiment (DOE) method is necessary. However, a large number of test trials would be needed to determine the relationships between the mechanical properties of MMNCs and the four processing parameters: ultrasonic power, processing temperature, time and nanoparticle weight percentage. The focus of this study is on the processing parameter optimization for nanocomposites with 1.0wt.% SiC nanoparticles. It was

determined that a processing time of 60 minutes was adequate to disperse 1.0wt.% nanoparticles in A356 melt. Thus, process optimization was simplified by focusing on optimizing the other two processing parameters: processing temperature and ultrasonic power. The processing temperature is important in that it affects the wettability, chemical reaction, and thus the bonding strength between the nanoparticle and the Al matrix. Considering all the influencing factors, three processing temperatures were selected for the DOE trials: 650 °C, 700 °C, and 760 °C. According to the ultrasonic system manufacturer, the full output of the transducer is 4.0 kW. In the preliminary experiments, ultrasonic dispersion was ineffective if ultrasonic power was lower than 2.2 kW. Thus three different powers were selected for the DOE trials: 2.5kW, 3.0kW, and 4.0kW. Therefore, the DOE trials were designed as 2 factors x 3 levels, which required a total of 18 trials (9 initial trials and one replica). Each trial produced four tensile bars to obtain tensile data. The tensile test results of DOE were summarized in Fig. 7 (a), as the processing temperature rises from 650 °C to 700 °C, both the ultimate tensile strength (UTS) and yield strength increase. However, with a processing temperature of 760 °C, the strength actually decreases. This could be due to more chemical reaction between the SiC nanoparticles and matrix alloy at that temperature. With regard to ultrasonic powers, best performance is achieved with a power of about 3.0 kW. With an ultrasonic power higher than 3.0 kW, the UTS and yield strength are not improved much. Moreover, the elongation of nanocomposites, as shown in Fig. 7(b), remains close to that of pure A356. Therefore, the optimized ultrasonic power and processing temperature are around 3.0 kW and 700 °C respectively. With those optimized parameters, and only 1.0 wt.% of SiC nanoparticles, the mechanical properties of nanocomposites are improved near 100% with little change in elongation.

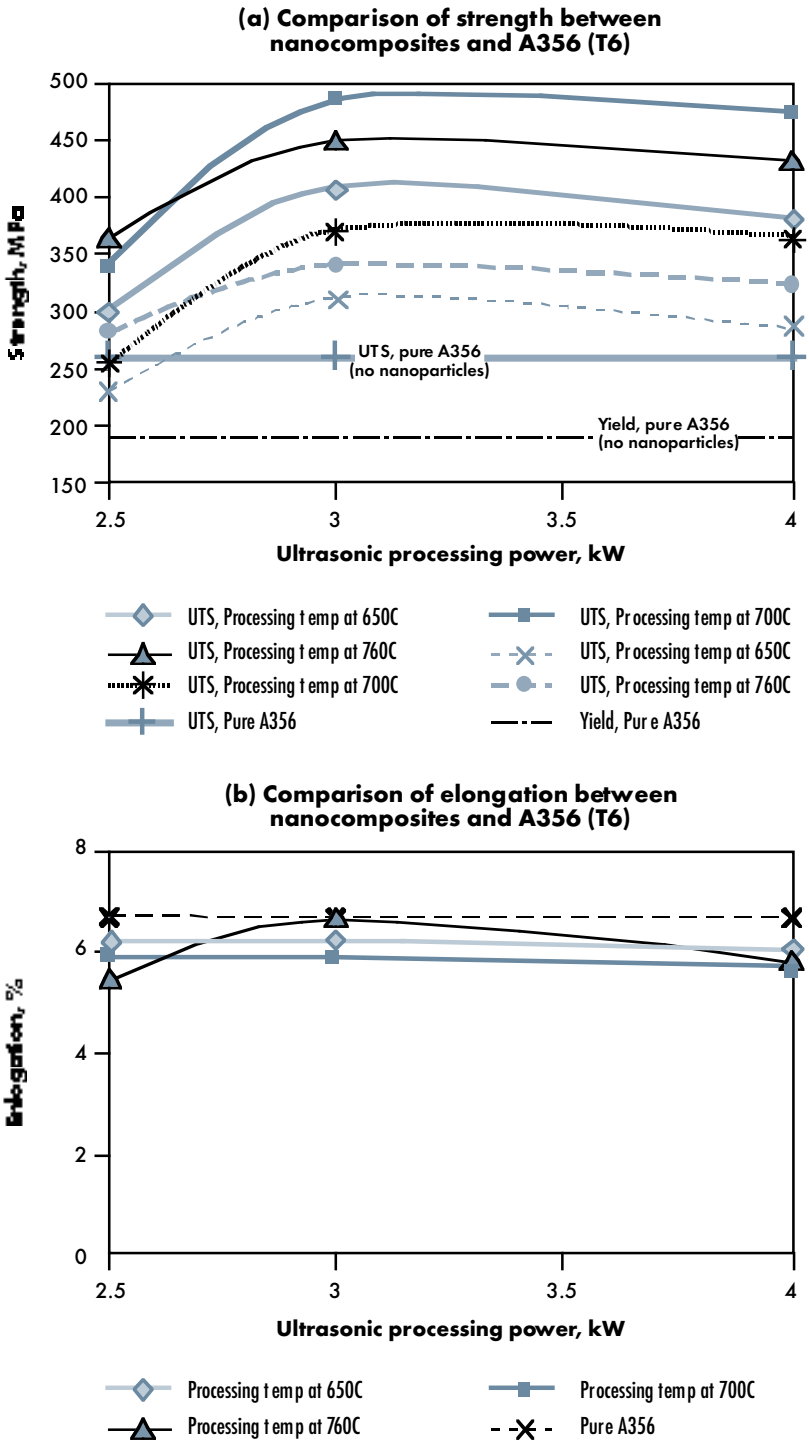

Fig. 7. Comparison between nanocomposite and A356

SEM

Samples of A356 matrix and nanocomposite after T6 heat treatment were examined by SEM, and typical results are shown in Fig.8. For the A356 matrix sample, the images clearly show _ Al phase and eutectic Si phase shown as white area in Fig.8 (a). Fig.8 (b) clearly shows that nano-sized SiC particles were uniformly distributed and effectively dispersed in the A356 matrix. It should be noted that some micro clusters still remain in the 5.3. TEM

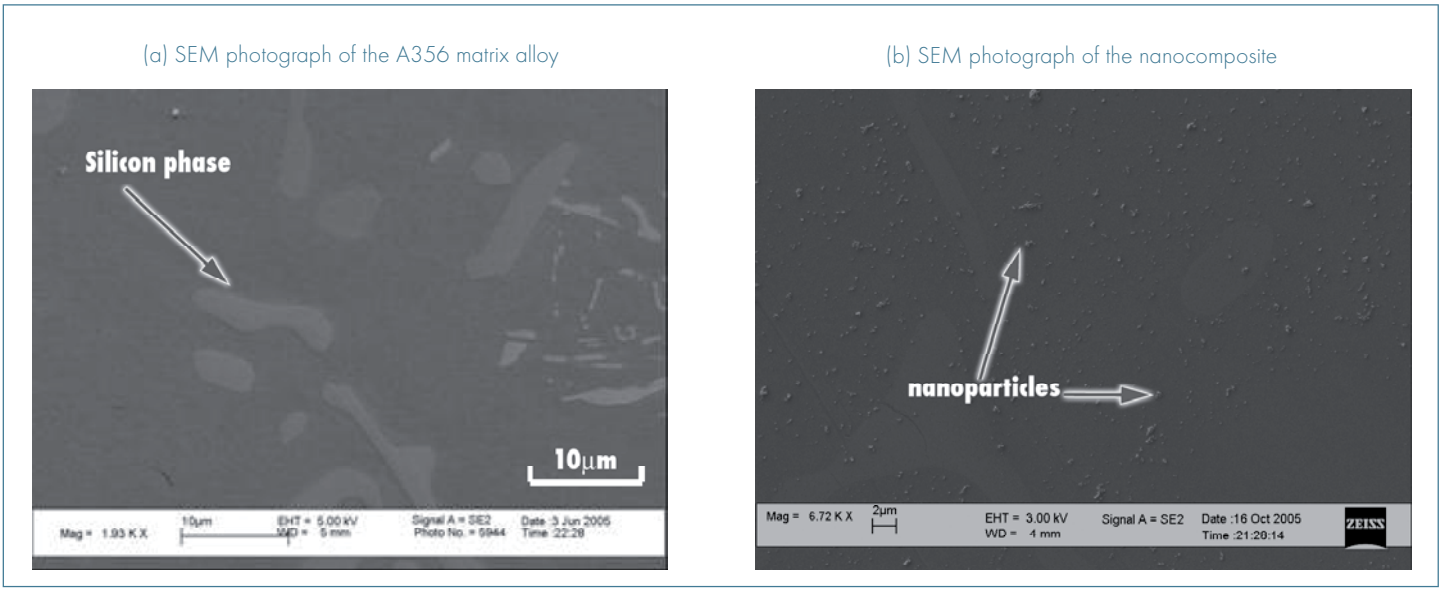

Fig. 8. SEM images of A356 alloy and nanocomposite

The nanostructures, lattice distortion around the nanoparticles, and the bonding interface between the nanoparticle and the matrix were studied by TEM. TEM samples were prepared with a focus ion milling (FIB) instrument, which can ease the preparation process significantly. First a piece of material was cut from the cast bulk MMNC, and mechanically polished to a foil of 50 μm thick with a surface finish of 50 nanometers. Then the thin foil was cut to a rectangle shape of 1.0mm¥2.0mm and glued to a partial nickel washer with a diameter of 3.0 mm. FIB (Zeiss CrossBeam) with a working distance of 5.23 mm and a voltage of 3.0 kV was used. The sample was first milled down to 15 μm deep, 54° tilt and with a milling current of 2.0 nA. A fine trapezoid was obtained and further refined to 300nm thickness with a milling current of 200 pA and then 50 pA. Finally, the sample was tilted to 60° and a milling current of 10pA was used until it was less than 100nm thickness.

Fig. 9 shows a typical bright-field TEM image of the nanocomposite. The image clearly shows the single particles were dispersed in the matrix. As expected, the nanoparticles were engulfed inside the grain. However, from the literature review, micro particles and even submicron particles are normally pushed to the grain boundary by the solidification front, which results in degradation in material ductility and other mechanical properties [23]. Selected Area Diffraction (SAD) was used

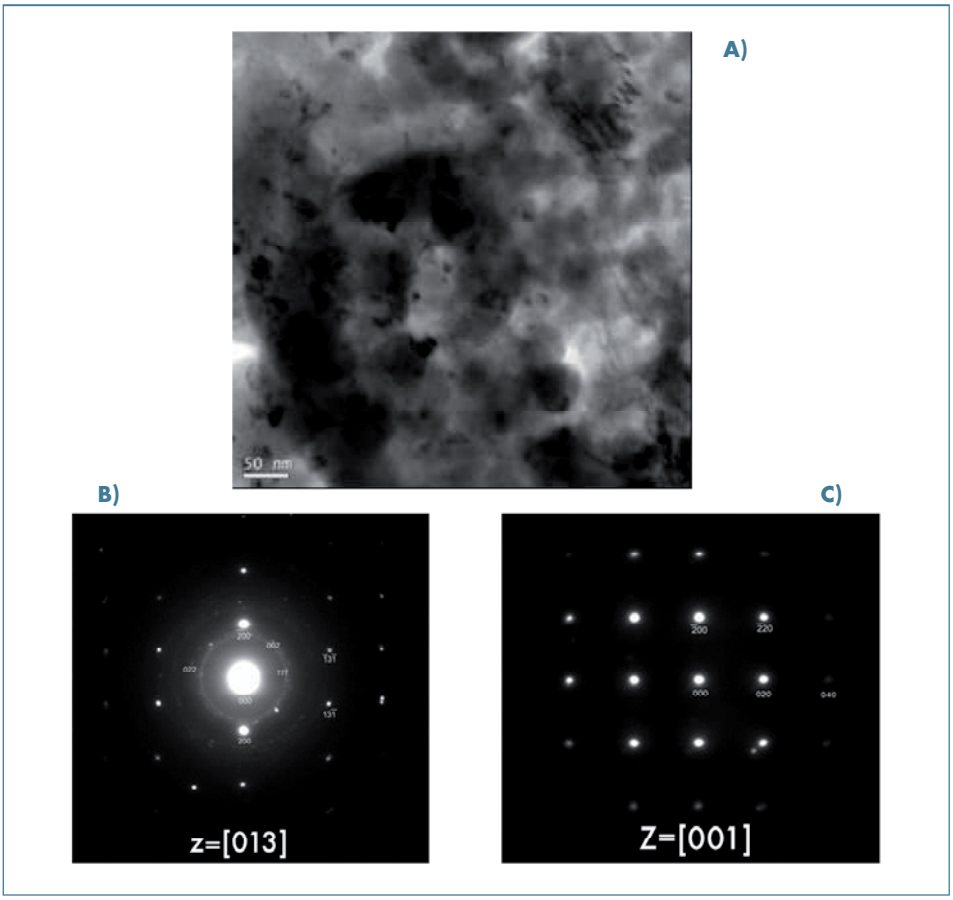

Fig. 9. (a) Bright Field TEM image of Al nanocomposite; (b) Selected Area Diffraction (SAD) of the nanocomposite; (c) Selected Area Diffraction (SAD) of the Al matrix only

to identify the phases. Fig. 9(b) clearly shows two sets of diffraction patterns, one is for the matrix Al index as zone axis [013] while the other ring set is for nanoparticles. Although the nanoparticles are single crystalline β-SiC, the diffraction pattern is concentric

circles, indexed as 111, 002, and 022, etc, due to the random orientation. The diffraction pattern suggests that no preferential crystal orientations exist for the reinforcement nanoparticles in the Al matrix. The diffraction pattern of the Al matrix only was also taken, as shown in Fig. 9(c) indexed as the zone axis [001] for comparison with that of the nanocomposite.

High Resolution transmission electron microscopy (HRTEM) can provide structural information at a spatial resolution better than 1 nm. In both the matrix and the reinforcement phase, the positions of individual atomic columns can be identified if it is tilted to the zone axis at a low index. In Fig.10, the lattice of the Al matrix is clearly shown. However it is very difficult to find a particle also oriented in a low index at the zone axis, making it impossible to reveal the lattices of the Al matrix and the nanoparticle simultaneously. Nevertheless, the image clearly shows that the lattice of Al gradually evolved to that of SiC, This gradual transition indicates no lattice distortions or mismatch, which could have been eliminated by the T6 treatment.

EDS IN TEM

In order to identify the composition of the nanoparticles locally, the high resolution EDS in TEM mode was used. The beam spot reduced to 9nm, which was small enough to focus on a single SiC nanoparticle. However, it should be noted that the electron beam and material interaction zone could be larger. Fig. 11 (a), (b) and (c) show the EDS spot spectra on the nanocomposite, the Al matrix and the SiC, respectively. As the beam focused on the nanocomposite with a bigger spot size, Si, C and Al were detected as strong peaks, and only Al peak appeared strong as the spot was focused on the Al matrix.

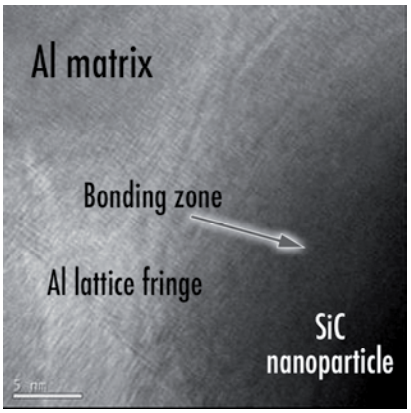

Fig. 10. BF HRTEM image of bonding zone around single particle in Al matrix at 850k Magnification

Moreover, as the beam was focused on a single SiC nanoparticle, the spectrum showed high peaks of Si and C and a low peak of Al element.

CONCLUSION

In this study, the feasibility of ultrasonic cavitation based dispersion of nanoparticles in A356 was theoretically studied and validated by analytical modeling, particularly for a simplified two-nanoparticle system in A356 melt.

An experimental system for ultrasonic cavitation based solidification processing was fully developed and alloy A356 nanocomposites were fabricated and characterized. With optimized processing parameters, the tensile test results showed that, with only 1.0wt% nano-sized SiC, the ultimate tensile strength (UTS) and Yield strength of the nanocomposites were

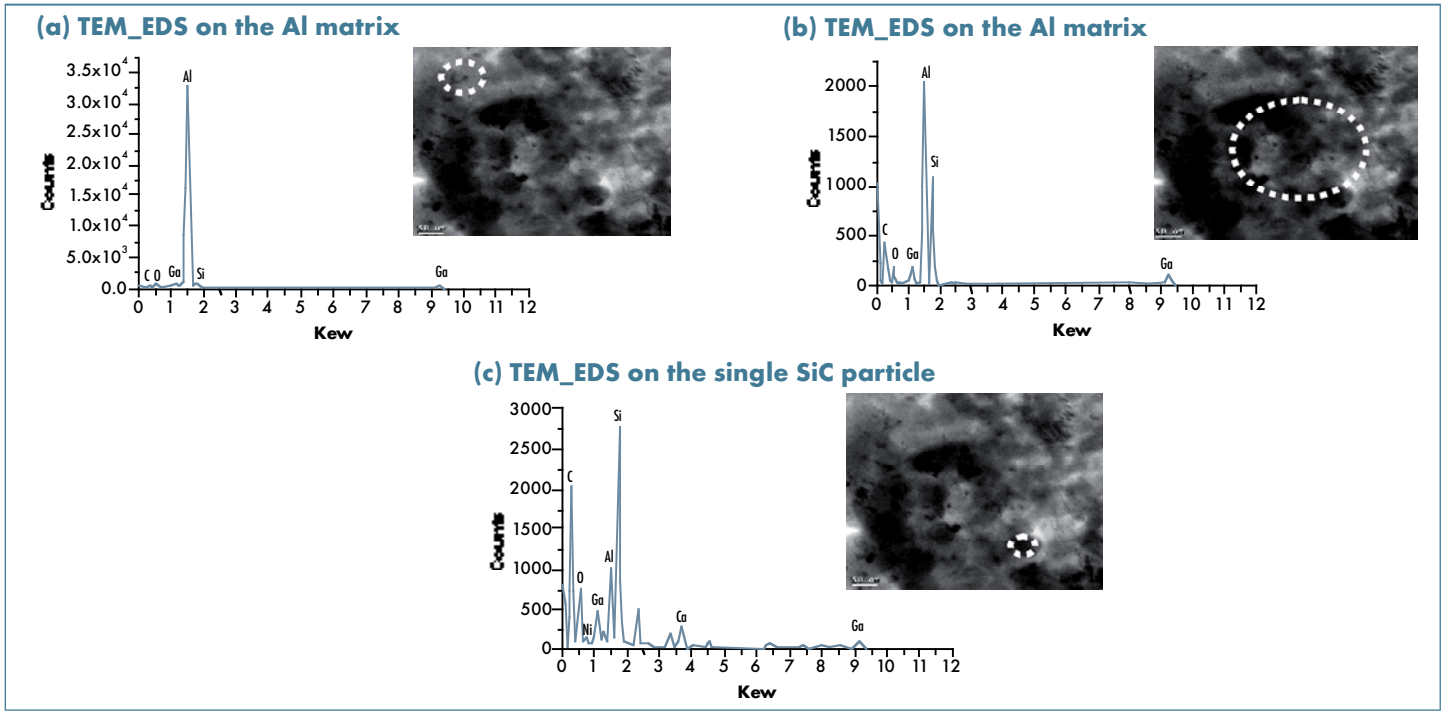

Fig. 11. EDS spectrum of the matrix, particle and composite in TEM mode

improved approximately 100% while ductility is retained.

Micro/nano structure study shows that good nanoparticle distribution and dispersion in the Al matrix were achieved. EDS in TEM showed that the processing was well protected from oxidation and single nanoparticle was clearly identified. By use of HRTEM, the nanostructure study indicates that a good bonding was obtained and the lattice of the Al matrix gradually evolved to that of the nanoparticles.

ACKNOWLEDGEMENTS

This work is supported by National Science Foundation and the American Foundry Society.

REFERENCES

[1] Q.C. Jiang, X.L. Li, and H.Y. Wang, Scripta Materialia, vol.48, (2003), 713.

[2] S. Rawal, JOM, vol.53, (2001), 14.

[3] N. Crainic, A.T. Marques, Key engineering materials, vol.230-232, (2002), 656.

[4] T. Yamasaki, Y.J. Zheng, Y. Ogino, M. Terasawa, T. Mitamura, T. Fukami, Materials Science and Engineering A, vol.350A, (2003), 168.

[5] S. Hirsosawa, Y. Shigemoto, T. Miyoshi, H. Kanekiyo, Scripta materialia, vol.48, (2003), 839.

[6] F. Audebert, F. Prima, M. Galano, M. Tomut, P.J. Warren, I.C. Stone, B. Cantor, Materials transitions, vol.43, (2002), 2017.

[7] X.C. Tong, H.S. Fang, Metallurgical and materials Transactions, vol.29A, (1998), 875.

[8] X.C. Tong, H.S. Fang, Metallurgical and materials Transitions, vol.29A, (1998), 893.

[9] FK Sautter, Journal of the electrochemical society, vol.110, (1963), 557.

[10] A.F. Zimmerman, G. Palumbo, K.T. Aust, U. Erb, Materials science and engineering A, vol.328, (2002), 137.

[11] F. Niu, B. Cantor, P.J. Dobson, Thin solid films, vol.320, (1998), 184-191.

[12] R.K. Islamgaliev, N.F. Yunusova, I.N. Sabirov, A.V. Sergueeva, R.Z. Valiev, Materials science and engineering A, vol.319, (2001), 877.

[13] R.J. Arsenault, L. Wang, C.R. Feng, Acta metal. Mater. Vol.39, (1990), 47.

[14] V.C. Nardone, K.M. Prewo, Scripta metallugica, vol.20, (1986), 43.

[15] S. Suslick, Y. Didenko, M.M. Fang, T. Hyeon, K.J. Kolbeck, W.B. McNamara, M.M. Midleleni, M. Wong, Phil. Tans. R. Soc. Lond., vol.A357, (1999), 335.

[16] A.R. Kennedy, A.E. Karantzalis, Materials Science and Engineering A, vol.264, (1999), 122.

[17] K. Bhanumurthy, R. Schmid-Fetzer, Composites A, vol.32, (2001), 569.

[18] A. Urenua, M.D. Escalera, L Gil, Journal of materials science, vol.37 (2002), 4633.

[19] O.V., Abramov, Ultrasound in Liquid and Solid Metals, Boca Raton, FL: CRC Press, 1994.

[20] L. Ma, F. Chen, G. Shu, Journal of materials science letters vol.14, (1995), 649.

[21] V. Laurent, D. Chatain, N. Eustathopoulos, Journal of materials science, vol.22, (1987), 244.

[22] Y. Yang, J. Lan, X. Li, Materials Science and Engineering A, vol.380, (2004), 378.

[23] G. Wilde, J.H. Perepezko, Materials Science and Engineering A, vol.283, (2000), 25.